3-1-2020

S-seco-porphyrazine as a new member of the seco-porphyrazine family – Synthesis, characterization and photocytotoxicity against cancer cells

Dariusz T. Mlynarczyk
Poznan University of Medical Sciences

Jaroslaw Piskorz
Poznan University of Medical Sciences

Lukasz Popenda
Uniwersytet im. Adama Mickiewicza w Poznaniu

Magdalena Stolarska
Poznan University of Medical Sciences

Wojciech Szczolko
Poznan University of Medical Sciences

See next page for additional authors

Bioorganic Chemistry 96 (2020) 103634

Contents lists available at ScienceDirect

Bioorganic Chemistry

journal homepage: www.elsevier.com/locate/bioorg

S-*seco*-porphyrazine as a new member of the *seco*-porphyrazine family – Synthesis, characterization and photocytotoxicity against cancer cells

Dariusz T. Mlynarczyk[a,1], Jaroslaw Piskorz[b,*,1], Lukasz Popenda[c], Magdalena Stolarska[a], Wojciech Szczolko[a], Krystyna Konopka[d], Stefan Jurga[c], Lukasz Sobotta[b], Jadwiga Mielcarek[b], Nejat Düzgüneş[d], Tomasz Goslinski[a,*]

[a] Department of Chemical Technology of Drugs, Poznan University of Medical Sciences, Grunwaldzka 6, 60-780 Poznan, Poland
[b] Department of Inorganic and Analytical Chemistry, Poznan University of Medical Sciences, Grunwaldzka 6, 60-780 Poznan, Poland
[c] NanoBioMedical Centre, Adam Mickiewicz University, Wszechnicy Piastowskiej 3, 61-614 Poznan, Poland
[d] Department of Biomedical Sciences, University of the Pacific, Arthur A. Dugoni Scholl of Dentistry, 155 Fifth Street, San Francisco, CA 94103, USA

ARTICLE INFO

Keywords:
Liposomes
NMR spectroscopy
Photodynamic therapy
Porphyrazine
Singlet oxygen
Tribenzoporphyrazine

ABSTRACT

An important subgroup within the porphyrazine (Pz) family constitutes *seco*-porphyrazines, in the chemical structure of which one pyrrole unit is opened in the oxidative process. So far, there are only limited data on *N-seco*- and C-*seco*-Pzs. Here, the synthesis of a novel member of the Pzs *seco*-family, represented by an S-*seco*-tribenzoporphyrazine analogue, 22,23-bis(4-(3,5-dibutoxycarbonylphenoxy)butylsulfanyl)tribenzo[b,g,l]-22,23-dioxo-22,23-*seco*-porphyrazinato magnesium(II), is reported, with moderate 34% yield. The new derivative was characterized using NMR spectroscopy, UV–Vis spectroscopy, and mass spectrometry. In the photochemical study performed following the indirect chemical method with 1,3-diphenylisobenzofuran, S-*seco*-Pz revealed a high singlet oxygen quantum yield of 0.27 in DMF.

Potential photocytotoxicity of S-*seco*-Pz was assessed *in vitro* on three cancer cell lines – two oral squamous cell carcinoma cell lines derived from the tongue (CAL 27, HSC-3) and human cervical epithelial adenocarcinoma cells (HeLa). In the biological study, the macrocycle was tested in its free form and after loading into liposomes. It is worth noting that S-*seco*-Pz was found to be non-toxic in the dark, with cell viability levels over 80%. The photocytotoxic IC_{50} values for free S-*seco*-Pz were 0.61, 0.18, and 4.1 μM for CAL 27, HSC-3 and HeLa cells, respectively. Four different liposomal compositions were analyzed, and the cationic liposomes revealed the highest photokilling efficacy, with the IC_{50} values for CAL 27, HSC-3, and HeLa cells at 0.24, 0.25, and 0.31 μM, respectively. The results of the photocytotoxicity study indicate that the new S-*seco*-tribenzoporphyrazine can be considered as a potential photosensitizer in photodynamic therapy of cancer, along with the developed cationic liposomal nanocarrier.

1. Introduction

Porphyrazines (Pzs) constitute a distinct group of porphyrinoid macrocycles and are often considered as synthetic analogues of porphyrins that exist in nature. They have gained increasing attention due to remarkable optical and electrochemical properties, which make them potential catalysts or materials for chemistry and technology, as well as photosensitizers for photodynamic therapy in medicine [1–3]. Light in the region 600–800 nm penetrates deeply human tissues and can initiate a photodynamic reaction in the presence of molecular oxygen and photosensitizer, leading to the generation of reactive oxygen species that are essential for photodynamic therapy [4–6].

Seco-porphyrazines (*seco*-Pzs) have gained much attention since their first synthesis by the laboratories of Professors A.G.M. Barrett and B.M. Hoffman in 1994 [7]. These compounds attracted interest because of their optical properties and high singlet oxygen generation quantum yields (up to 0.74) [8]. It is notable that when one pyrrole unit of the porphyrazine is opened in an oxidative process, giving access to its *seco*-porphyrazine derivative, singlet oxygen generation may increase. There are only a few *seco*-porphyrazines described in the literature, among

* Corresponding authors at: Department of Inorganic and Analytical Chemistry, Poznan University of Medical Sciences, Grunwaldzka 6, 60-780 Poznan, Poland (J. Piskorz). Department of Chemical Technology of Drugs, Poznan University of Medical Sciences, Grunwaldzka 6, 60-780, Poznan, Poland (T. Goslinski).
E-mail addresses: piskorzj@ump.edu.pl (J. Piskorz), tomasz.goslinski@ump.edu.pl (T. Goslinski).
[1] Authors declare equal contribution.

https://doi.org/10.1016/j.bioorg.2020.103634
Received 21 October 2019; Received in revised form 7 January 2020; Accepted 28 January 2020
Available online 30 January 2020

them N-*seco*-porphyrazines [7–15] and C-*seco*-porphyrazines [16–21], synthesized from diaminomaleonitrile and maleonitrile, respectively. Worth mentioning are also three-quarter Pzs, technically accounted as *seco*-Pzs, in which one of the pyrrole rings is not formed at all during synthesis; therefore, we would suggest calling them – *sine*-Pzs (*sine* – *Lat.* without) [22,23]. Moreover, quite structurally close derivatives are Pzs in which at least one of the pyrrole β-carbons is lost during macrocyclic pyrrole oxidation [24]. It seems that the low number of *seco*-Pzs published so far may be attributed to their limited stability and/or the oxidation feasibility of pyrrolic rings. Another aspect might be related to their difficult isolation and low reaction yields during their formation (even 0.3%) [23]. In addition, the mechanistic aspects of their synthesis have not been fully explained at the experimental level. Not much is also known about the reactivity of *seco*-porphyrazines. Their high photoactivity has been analyzed so far in photocatalytic oxidation, the cycloaddition of oxygen to 1,3-dienes [25] on a polymeric solid support [14]. In addition, Prof. P.A. Stuzhin, in a study published with A.V. Kozlov, presented the transformation of *N-seco*-Pz towards a novel porphyrinoid, named pyraziniporphyrazine, in which pyrrole was expanded to a pyrazine ring [10]. Interestingly, methodologies developed in Professors A.G.M. Barrett and B.M. Hoffman groups by Montalban *et al.* and Sakellariou *et al.* allowed the further oxidation of *seco*-porphyrazines to di*seco*-porphyrazines, with the *trans* isomer reported to be stable long enough that it could be isolated [12,15]. Moreover, Gonca presented interesting 4-biphenylyl C-*seco*-Pz complexes in the free form and after metallation with Fe(III), which gave further access to monomacrocyclic complexes with pyridine or polymacrocyclic complexes with pyrazine [19,21].

Porphyrazines substituted with sulfanyl moieties have also been studied widely. They can be modified, have interesting optical [26,27] and electrochemical properties [28–30], and have the potential to be used in photodynamic therapy (PDT) [31,32] and wastewater treatment [33–35]. Although sulfanyl porphyrazines have been synthesized for over twenty years, S-*seco*-porphyrazine has never been reported and characterized so far [36]. Nevertheless, it should be pointed out that in 1992 Velázquez *et al.* reported the formation of porphyrazine-like macrocyclic compounds during the synthesis of sulfanyl porphyrazines, but unfortunately, they did not manage to isolate and characterize them [37].

Now, we report the first S-*seco*-Pz synthesis. The macrocycle was characterized using one and two-dimensional NMR techniques, UV–Vis spectroscopy, and mass spectrometry. After the quantum yield of singlet oxygen generation was established, the photocytotoxicity of *seco*-porphyrazine was evaluated *in vitro* against oral squamous cell carcinoma cell lines derived from the tongue (CAL 27, HSC-3) and human cervical epithelial adenocarcinoma cells (HeLa).

2. Results and discussion

2.1. Synthesis and identification

Attempts to cleave the ester groups present in tribenzoporphyrazine **1** following phase transfer conditions in a two-phase mixture of aqueous sodium hydroxide solution and dichloromethane led to a limited amount of a new blue product **2**, which was more polar than **1** in TLC chromatography, using dichloromethane/methanol mixtures (Scheme 1). The new molecule was soluble in chloroform, dichloromethane, tetrahydrofuran, toluene, *N*,*N*-dimethylformamide (DMF), dimethylsulfoxide (DMSO) and acetone, but was insoluble in *n*-hexane, methanol, and water. The UV–Vis spectrum of **2** was different from that observed for substrate **1** (Fig. 2). The split in the Q-band absorption of Pzs is the result of the loss of symmetry during demetallation, or, less commonly, the modification of the macrocyclic ring structure [1,3,38]. Moreover, MS ESI results indicated the formation of the oxidation product, as the monoisotopic mass signal of **1** increased by the mass of dioxygen (*m/z* found: 1279.368, $[M+H]^+$, $C_{68}H_{71}MgN_8O_{12}S_2$ requires 1279.448). A combination of these two measurements suggests the oxidative breaking of the pyrrole ring and S-*seco*-porphyrazine formation (Scheme 1).

The yield of the above-discussed reaction was very low (< 5%). Therefore, suspecting *seco*-Pz formation, known literature approaches developed so far for the synthesis of *seco*-Pzs were studied for scaling-up the synthesis from **1** to **2**. The literature survey indicated that *seco*-Pz formation has been achieved as the result of the following processes: (*i*) in the macrocyclization reaction as a byproduct [15,22,23]; (*ii*) after the oxidation reaction using: (*a*) $KMnO_4$ [8,11,15], (*b*) MnO_2 [15], (*c*) gaseous oxygen [10], and (*d*) oxygen from air [12–14]; (*iii*) in the demetallation reaction with acetic or trifluoroacetic acid in an air atmosphere [7,15,17,18] or in an inert gas atmosphere [16–18,20,21]; (*iv*) serendipitously in non-specific reactions – loss of both β-carbons of one pyrrole during attempted metallation of β,β-dihydroxyporphyrazine derivative with nickel(II) [24], or in a specific one-pot reaction leading to multi-gram yields of a water-soluble *N-seco*-Pz [9].

Attempts to find suitable conditions for the synthesis of the desired S-*seco*-Pz **2**, taking into account the reaction conditions given above, led to interesting observations. The oxidation reaction of **1** with MnO_2 in dichloromethane or 2,3-dichloro-5,6-dicyano-1,4-benzoquinone (following conditions given in Ref. [39]) did not lead to any *seco*-product at all, and enabled the isolation of only the unreacted substrate. Once the substrate was treated with trifluoroacetic acid, only demetallated Pz **3** was isolated. Finally, the biphasic system consisting of the aqueous solution of $KMnO_4$ and dichloromethane led to **2** in moderate 34% yield (Scheme 1).

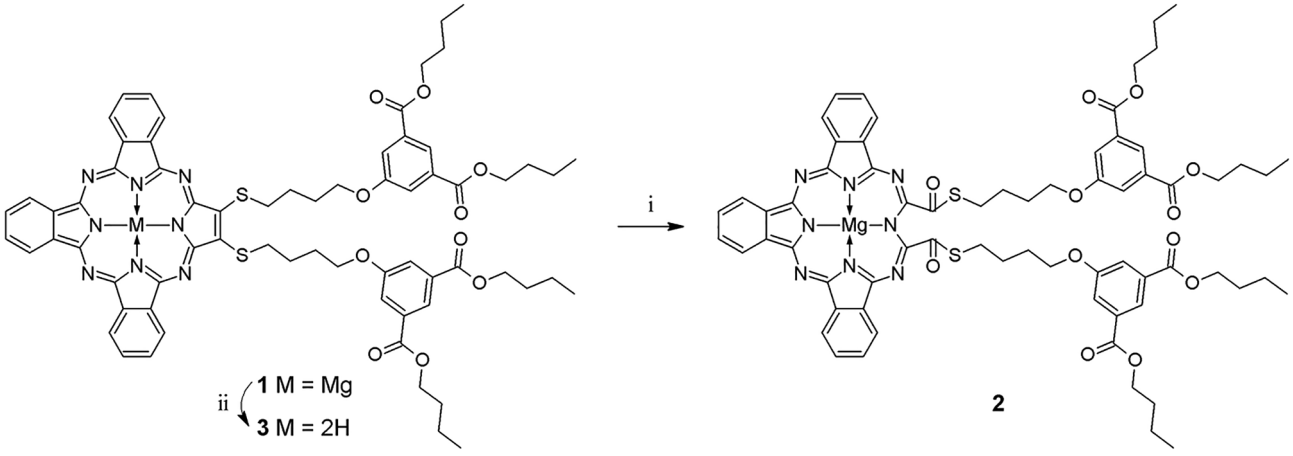

Scheme 1. Reactivity of **1**: (i) $KMnO_4$, H_2O/dichloromethane 1:1 (v/v), 2 h, room temperature; (ii) trifluoroacetic acid, 15 min., room temperature, air.

Initially, we attempted to obtain **2** in its crystal form. When all attempts to obtain the single crystal suitable for crystallographic measurements failed, the structure was analyzed with the use of NMR spectroscopy and MS spectrometry. Therefore, a series of 1D (^{1}H, ^{13}C) and 2D (^{1}H-^{1}H COSY, ^{1}H-^{1}H TOCSY, ^{1}H-^{1}H NOESY, ^{1}H-^{13}C HSQC and ^{1}H-^{13}C HMBC) accompanied by 1D ^{1}H temperature spectra ranging from –15 to 55 °C, were recorded.

These experiments were conducted mainly for Pz **2** structure verification, but initially due to obtaining far more complex spectra than expected, it was necessary to examine whether the macrocycle **2** in pyridine-d_5 solution exists in its free form only or is involved in stacking or aggregation. The NMR data obtained in pyridine-d_5 revealed that Pz **2** is not aggregated during the measurement as no significant differences were observed in the temperature spectra. Also, experiments in DMSO-d_6 or $CDCl_3$ with the addition of CF_3COOD did not lead to spectra with better spectral quality. In addition, NMR data revealed that the proton (and carbon) signals assigned to each of the 3,5-dibutoxycarbonylphenoxy substituents appear at similar but slightly shifted values at 0.76, 1.19, 1.42, 4.12, 8.03, 7.86 ppm, and 0.85, 1.34, 1.61, 4.32, 8.26, 8.51 ppm, respectively (see Fig. 1). The resonances of non-terminal protons belonging to both substituents and present in the butyl linker appeared at 1.31–1.22 ppm. Trying to explain these phenomena, we analyzed the ^{1}H, ^{13}C NMR spectroscopy and X-ray data presented by Montalban *et al.* for 2,3,7,8,12,13,17,18-octakis(dimethylamino)-2-*seco*-porphyrazine-2,3-dione, [2,3-bis(dimethylamino)-7,8,12,13,17,18-hexapropyl-2-*seco*-2,3-dioxoporphyrazinato]zinc(II), as well as the ^{1}H, ^{13}C NMR spectroscopy data of [2,3,7,8,12,13,17,18-octakis(dimethylamino)-2,12-di*seco*-2,3,12,13-tetraoxoporphyrazinato)zinc(II) [15]. According to the NMR data that have been presented for these three macrocycles, it could be concluded that the *seco*-substituents undergo rotation, causing the signals belonging to both substituents to appear separately. Characteristic for *seco*-carbonyl carbon resonance, the presence of which proves the opening of the pyrrole ring in the ^{13}C NMR spectrum, was observed at 167.96 ppm. No correlations of this signal with any of the isophthalate nor aliphatic ester proton resonances were found in the ^{1}H-^{13}C HMBC spectrum, unlike the adjacent peak at 167.36 ppm assigned to isophthalate carbonyl groups, which allowed correct identification of these two signals (see Figs. S01 and S02 in the Supplementary Information for the ^{1}H and ^{13}C NMR spectra, respectively).

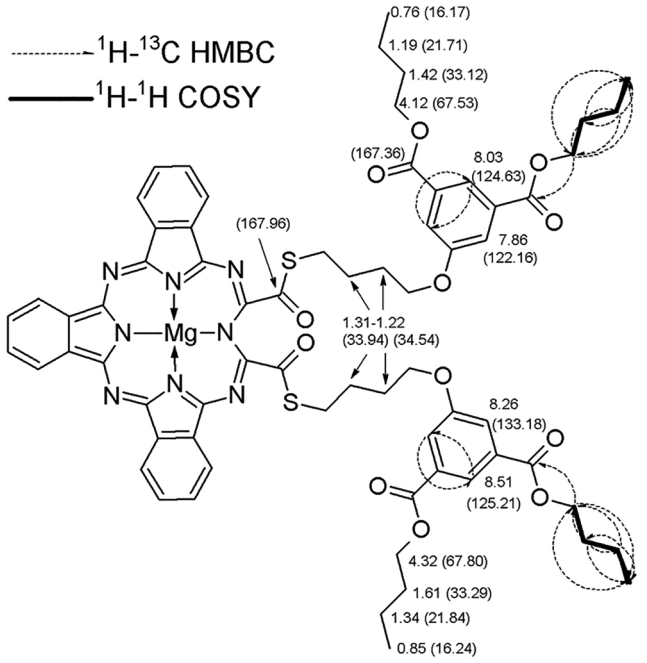

Fig. 1. ^{1}H and (^{13}C) chemical shift values [ppm] of Pz **2**. Selected ^{1}H-^{1}H COSY and ^{1}H-^{13}C HMBC correlations are marked with bold lines and dashed arrows, respectively. The ^{13}C chemical shift values are presented with two decimal places.

As we mentioned before, the initial MS ESI results indicated the formation of the oxidation product, as the monoisotopic mass signal of **1** increased by the mass of dioxygen. This result was confirmed in another MS study using the MS MALDI TOF technique (*m/z* found: 1279.3926, $[M+H]^+$, $C_{68}H_{71}MgN_8O_{12}S_2$ requires 1279.4483). Analysis of the Pz **2** MS MALDI spectrum, accompanied by the linked scan technique revealed a series of fragmentation signals that confirmed the structure of *seco*-porphyrazine. The most significant signal at *m/z* 517.143 corresponds to the fragmentation ion formed by the break of both bonds between *seco*-carbonyl carbons and sulfur atoms (see Supplementary Information). The formation of such species was possible only when the oxidation of the pyrrole carbons to the *seco*-carbonyl groups had occurred. Additionally, the mass spectrum revealed a series of *m/z* fragmentation peaks confirming the structure of S-*seco*-tribenzoporphyrazine **2** (for the MS spectra see Figs. S06–S09 in the Supplementary Information**)**.

2.2. Photophysical characterization

The B-band and the Q-band are the characteristic absorption bands in the UV–Vis spectra of porphyrazine compounds [40]. *Seco*-Pz is a compound composed of three pyrrole rings linked together to form a macrocyclic ring, which results in significant differences in the Q-band absorption of *seco*-Pz (**2**) in comparison to the parent porphyrazine **1** [1]. The Q-band split in the recorded absorption spectrum was also observed for demetallated Pz **3**, but to a lesser extent than for **2**. The decrease in symmetry and the resulting Q-band splitting in the spectra of both molecules **2** and **3** were, however, caused by different factors. In the case of **2** it was an effect of the oxidation of one pyrrole ring within the macrocycle, whereas for **3** it was a result of demetallation.

The ability to generate singlet oxygen by the *seco*-Pz **2** was assessed using the indirect chemical method with DPBF and ZnPc as a reference. The results of this photochemical experiment revealed that **2** is a moderate singlet oxygen generator with the quantum yield of singlet oxygen generation equal to 0.27 in DMF. Macrocycle **1** under the same conditions had a quantum yield of only 0.05 [41]. Therefore, the pyrrole ring-opening caused a five-fold increase of the singlet oxygen quantum yield.

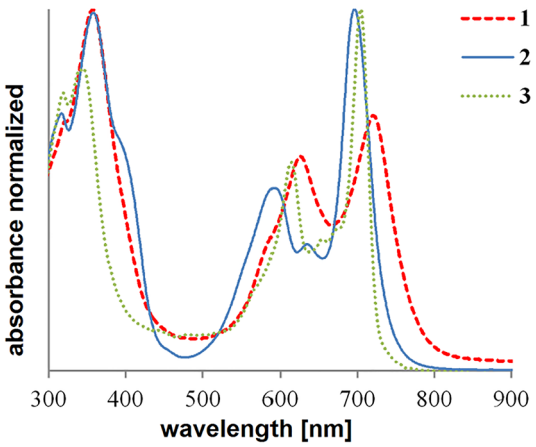

Fig. 2. UV–Vis spectra of **1** (dashed line), **2** (solid line), and **3** (dotted line). All spectra were recorded in dichloromethane and are normalized.

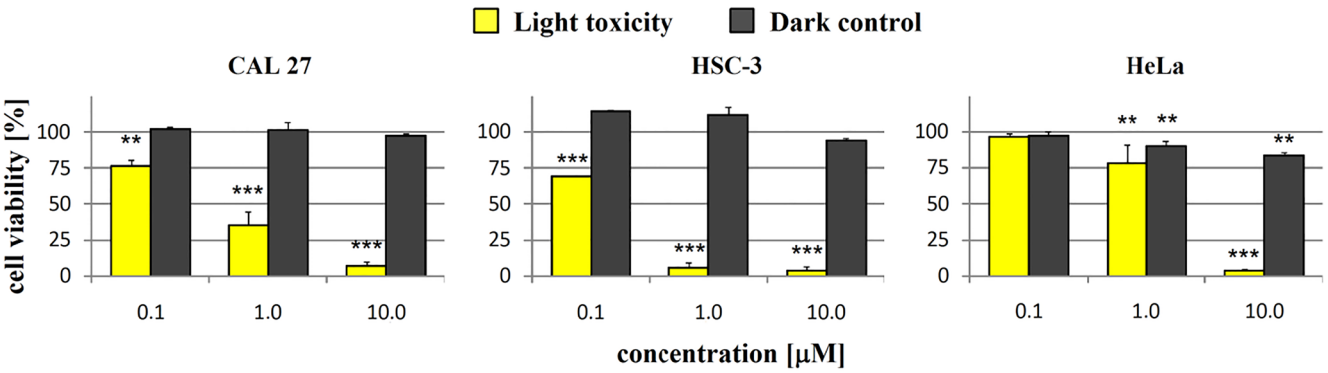

Fig. 3. Light toxicity (cell viability as % of untreated controls) and dark control (cell viability as % of untreated controls) of **2** against CAL 27, HSC-3 and HeLa cells. Data represent the mean ± standard deviation obtained from experiments performed in triplicate. Statistical significance is indicated with asterisks: *p < 0.05, **p < 0.01, ***p < 0.001.

2.3. Biological activity against cancer cell lines

The potential application of **2** in the photodynamic therapy of cancer was evaluated by *in vitro* examination of its photocytotoxicity on two oral squamous cell carcinoma cell lines derived from the tongue (CAL 27, HSC-3) and human cervical epithelial adenocarcinoma cells (HeLa). Firstly, the dark toxicity of **2** was tested at the concentrations of 0.1, 1.0, and 10 μM. There was no significant dark toxicity to the oral cancer cells. However, some cytotoxicity on cervical epithelial adenocarcinoma cells was found at 1.0 and 10 μM, but the reduction in cell viability did not exceed 20% (Fig. 3 and Table S03 in the Supplementary Information). Thus, the light-induced toxicity was examined at the same concentrations. After 24 h of incubation with **2** dissolved in medium with 0.25% DMSO, cancer cells were exposed to light of 690 nm from a High Power LED Multi-Chip Emitter (*Roithner Lasertechnik GmbH*) for 20 min. On the next day, the cell viability was quantified by the Alamar Blue assay. It was found that at 0.1 μM *seco*-Pz **2**, CAL 27 and HSC-3 cell viability was reduced by about 30%, while there was no cytotoxicity to HeLa cells. *Seco*-Pz **2** at 1.0 μM had considerable photocytotoxicity to CAL 27 and HSC-3 cells, with reduction in viability of 74% and 94%, respectively, but HeLa cell viability was reduced by only 22%. At the highest concentration (10 μM), photocytotoxicity of more than 90% was observed in all three cell lines tested (Fig. 3 and Table S03 in supplementary information).

Further studies were performed with liposomes to improve the aqueous solubility of *seco*-Pz **2** and its delivery to cancer cells. Liposomal nanoparticles have already been widely researched as a drug delivery system for photosensitizers [42,43]. Tribenzoporphyrazine **2** was incorporated into four different liposomes comprising 1-palmitoyl-2-oleoyl-*sn-glycero*-3-phosphocholine (POPC) or 1,2-dioleoyl-*sn-glycero*-3-phosphoethanolamine (DOPE), with either a negative charge (by the incorporation of L-α-phosphatidyl-DL-glycerol; PG) or a positive charge (by the inclusion of 1,2-dioleoyl-3-trimethylammonium propane; DOTAP). POPC is a phosphatidylcholine derivative with saturated palmitoyl and monounsaturated oleoyl chains, whereas DOPE belongs to phosphatidylethanolamines and possesses two unsaturated oleoyl chains (Fig. 4). Noteworthy, phosphatidylcholine and phosphatidylethanolamine derivatives are the most common phospholipids building mammalian cell membranes. Thus, lipid-based nanoparticles containing PC and PE, including liposomes, exhibit high biocompatibility and biodegradability, and are commonly used as carriers for the delivery of various drugs [44,45].

Liposomes with **2** and free liposomes without photosensitizer (as controls) were prepared by a thin-film hydration method and extruded through polycarbonate membranes to produce a uniform size distribution [32,46]. The mean diameter of the extruded liposomes with **2** varied from 0.16 to 0.41 μm. The size of liposomes was strongly dependent on the adjuvant lipid providing the net surface charge.

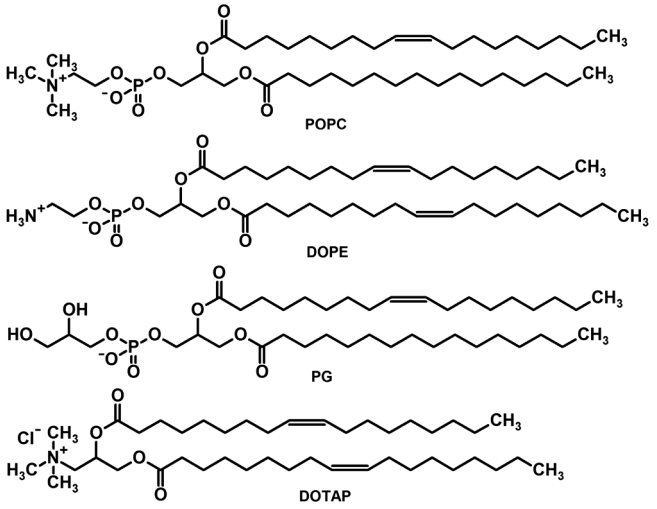

Fig. 4. Structures of lipids used for liposome preparation.

Positively charged liposomes with DOTAP had a mean diameter of 0.40 and 0.41 μm for **2**:DOTAP:POPC (0.1:2:8) and **2**:DOTAP:DOPE (0.1:2:8), respectively. By contrast, negatively charged liposomes with PG were smaller, with the mean diameter of 0.16 μm for **2**:PG:POPC (0.1:2:8) and 0.18 μm for **2** PG:DOPE (0.1:2:8). Noteworthy, POPC or DOPE, which constituted about 80% of the lipids in each liposomal formulation, did not have such a strong influence on the size of the liposomes, but POPC-containing particles were always a little smaller than the corresponding DOPE liposomes (Table S04 in Supplementary Information).

Liposomal formulations were examined at the same concentrations as those of the free form **2** in solution (0.1, 1.0 and 10.0 μM, Fig. 5 and Table S05 in Supplementary Information). Negatively charged PG:POPC liposomes with incorporated **2** had a photocytotoxic effect on all three cell lines only at 10 μM. The cell viability was reduced by about 20% for CAL 27 and HeLa cells, but was reduced by 50% in the case of HSC-3 cells. We should note that free **Pz 2** was about 10-fold more effective at this concentration, as well as at lower concentrations. Thus, encapsulation in these particular liposomes was inhibitory to the phototoxicity of **Pz 2**. This observation is in contrast to that described earlier for the magnesium(II) diazepinotribenzoporphyrazine in Piskorz et al. (2014) [47]. Therefore, optimal liposome compositions should be explored for the encapsulation of novel photosensitizers.

Cationic **2**:DOTAP:POPC particles showed higher activity. CAL 27 cell viability was reduced by 85% at the 1 μM concentration, and more than 99% at 10 μM. The viability of HSC-3 and HeLa cells was affected even at the lowest concentration (0.1 μM), by 22% and 26%

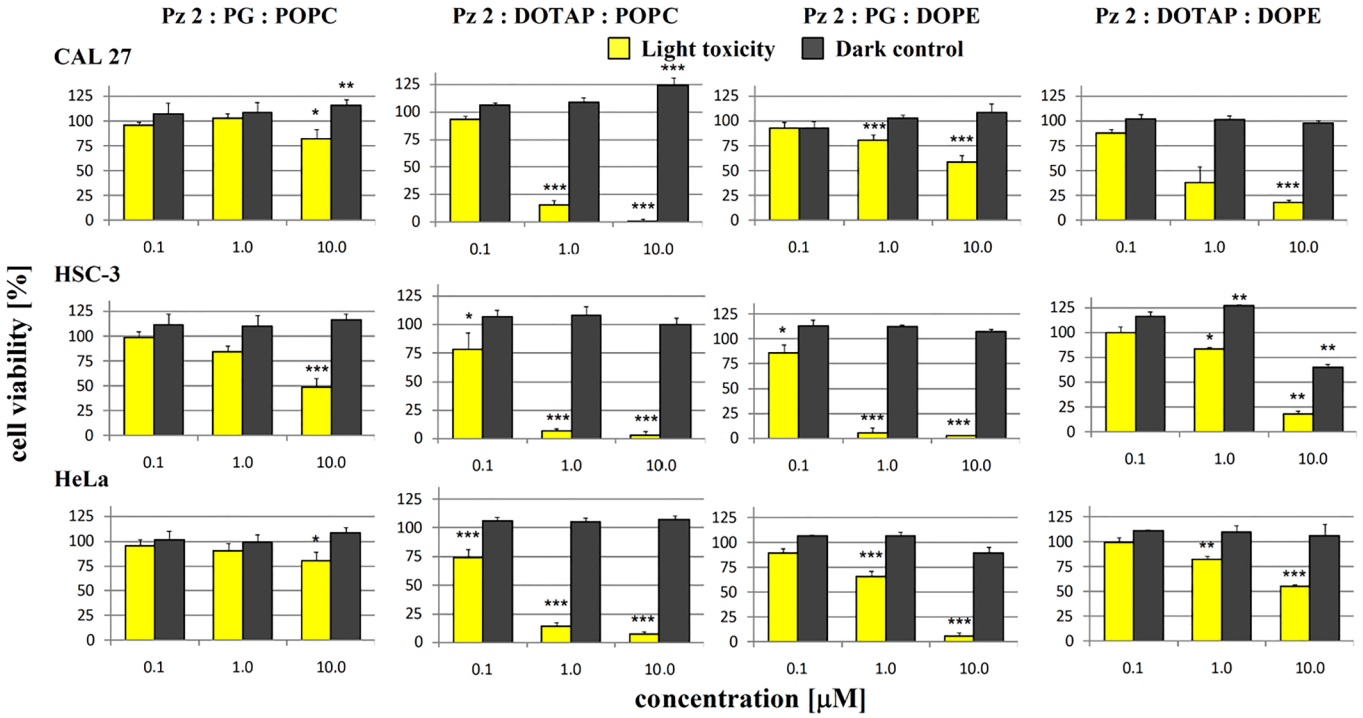

Fig. 5. Light toxicity (cell viability as % of untreated controls) and dark control (cell viability as % of untreated controls) of **2** in various liposomes against CAL 27, HSC-3 and HeLa cells. Data represent the mean ± standard deviation obtained from experiments performed in triplicate. Statistical significance is indicated with asterisks: *p < 0.05, **p < 0.01, ***p < 0.001.

respectively. Photocytotoxicities of 93% for HSC-3 and 86% for HeLa cells were found at 1 μM, whereas 10 μM **2** reduced HSC-3 and Hela cell viability by more than 90%. Another liposome formulation that was composed of **2**, PG and DOPE, reduced CAL 27 cell viability by about 20% at 1 μM, and more than 40% at 10 μM. HSC-3 cells were more sensitive, with the photocytotoxic effect of **2**:PG:DOPE reaching 94% and 97% at 1 and 10 μM, respectively. HeLa cell viability was affected by 34% at 1 μM and 94% at 10 μM. Positively charged **2**:DOTAP:DOPE particles revealed a photocytotoxic effect at 1 and 10 μM only. HSC-3 and HeLa cell viabilities were reduced by almost 20% at 1 μM. At the highest concentration (10 μM), photocytotoxicity to CAL 27 and HSC-3 cells exceeded 80%, whereas HeLa cell viability was reduced by only 45%. However, that concentration of **2**:DOTAP:DOPE liposomes also caused a significant dark cytotoxic effect on HSC-3 cells of about 35% (Fig. 5 and Table S05 in supplementary information).

Further examination aimed to compare the photocytotoxicity of free tribenzoporphyrazine **2** with that of the most effective liposomes composed of **2**, DOTAP and POPC. These experiments were performed at six concentrations of **2**, both free and incorporated into DOTAP:POPC liposomes, to determine the correlation between the viability of the cancer cells and the concentration of photosensitizer (Fig. 6 and Tables S06, S07 in Supplementary Information). The calculated IC_{50} values are presented in Table 1. S-*seco*-tribenzoprophyrazine **2** in its free form in solution exhibited the highest photocytotoxicity against HSC-3 cells with an IC_{50} value of 0.18 μM. By contrast, HeLa cells were the least sensitive to treatment with **2** (IC_{50} = 4.1 μM). After incorporation of **2** into DOTAP:POPC liposomes, its effect on all three cell lines was similar, with IC_{50} values in the range of 0.24–0.31 μM. It should be noted that liposomes enhanced the activity of **2** on HeLa cells more than 10 times, and on CAL 27 cells almost 3 times. The photocytotoxicity of **2**:DOTAP:POPC liposomes on HSC-3 cells, however, was slightly worse than those of the free form of **2** (Table 1).

Moreover, these results can be compared with the previous ones for the precursor compound tribenzoporphyrazine **1**, whose activity was examined on CAL 27 and HSC-3 cells [41]. It is worth emphasizing that

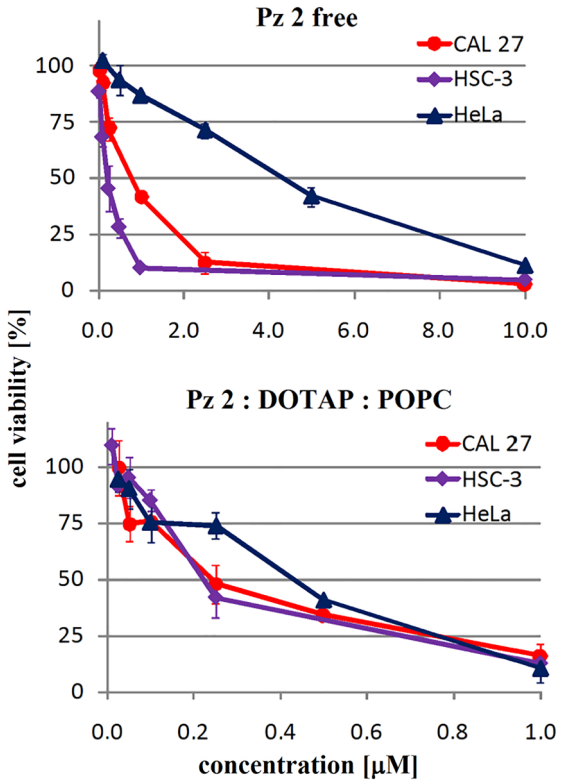

Fig. 6. Photocytotoxic effect of **2** in free form and encapsulated in DOTAP:POPC liposomes. Data represent the mean ± standard deviation for experiments performed in triplicate. Note the different scales of the x-axis.

S-*seco*-tribenzoporphyrazine **2** was much more active on both cell lines than tribenzoporphyrazine **1** with an IC_{50} value almost 11 times lower for CAL 27 cells and almost 60 times lower for HSC-3 cells.

Table 1
IC_{50} values [μM] for the cytotoxicity of **1** and **2**, free and after incorporation in DOTAP:POPC liposomes. Singlet oxygen generation quantum yields of **1** and **2**.

Photosensitizer	Cell lines			Φ_Δ (in DMF)
	CAL 27	HSC-3	HeLa	
1	6.66[a]	10.6[a]	–	0.05[a]
1:DOTAP:POPC	0.26[b]	0.19[b]	0.29[b]	–
2	0.61	0.18	4.1	0.27
2:DOTAP:POPC	0.24	0.25	0.31	–

[a] Value from reference [41].
[b] Value from reference [32].

Interestingly, after incorporation of **1** into DOTAP:POPC liposomes, the IC_{50} values were in the range of 0.19–0.29 μM and were similar to those obtained for **2**:DOTAP:POPC (0.24–0.31 μM, Table 1). However, the best results both for the free form and liposomal formulations, with IC_{50} values in the range 0.007–0.042 μM, have been previously found for 22,23-bis{4-[3,5-di(hydroxymethyl)phenoxy]butylsulfanyl}tribenzo [*b*,*g*,*l*]porphyrazinato magnesium(II), which formally is the derivative of **1** subjected to the reduction reaction, and thus equipped with the terminal hydroxymethyl groups [32,41].

The photocytotoxicity of other photosensitizers has also been assessed on CAL 27, HSC-3 and HeLa cell lines. Clinically approved 5-ALA (5-aminolevulinic acid) is enzymatically, intracellularly, converted to Protoporphyrin IX, which was found active *in vitro* against CAL 27 cells with IC_{50} values equal to 620 μM after irradiation for 50 s with 635 nm light (~18 mW/cm^2, 10 J/cm^2) [48]. Another popular photosensitizer, Chlorin e6, was found to act efficiently on the CAL 27 cell line with IC_{50} value equal to 1.06 μM after irradiation with a 0.5 J/cm^2 dose of 665 nm light [49]. The clinically relevant compound, porfimer sodium, better known in clinical practice as Photofrin®, was tested on HeLa cells. In the experiments, the IC_{50} values reached for Photofrin® were 2.57 μM when a light-dose of 5 J/cm^2 was used [50]. Lapshina et al. studied the photocytotoxicity of poly(*N*-vinylpyrrolidone) solutions of substituted phthalocyanines in HeLa human adenocarcinoma cells, which was characterized by the IC_{50} values of up to 1.83 μM after irradiation with a 8 mW/cm^2 dose of 670 nm light for 30 min [51]. Boron-dipyrromethenes (BODIPY) are gaining nowadays more attention in the photosensitizer field. One such molecule, comprising of oxovanadium(IV) complex bound to a boron-dipyrromethene moiety, was tested on HeLa cells, yielding IC_{50} equal to 0.15 μM when light from the range of 400–700 nm with 10 J/cm^2 dose for 1 h was applied [52]. Other significant results found in reviews (i.e. [53]) indicate that, although, it seems problematic to compare the results obtained at various light dosimetry parameters, the potential value of liposomal formulations of **1** and **2** for further photocytotoxicity studies towards photodynamic therapy, is high.

3. Experimental

3.1. Materials and instruments

All reactions were conducted in oven-dried glassware under an argon atmosphere using *Radleys Heat-On™* heating system. Solvents and all reagents were obtained from commercial suppliers and used without further purification, except for dichloromethane, which was freshly distilled before use. All solvents were removed by rotary evaporation at or below 50 °C. Dry flash column chromatography was carried out on *Merck silica gel 60*, particle size 40–63 μm, and reverse phase *Fluka C18 silica gel 90*. Thin-layer chromatography (TLC) was performed on silica gel *Merck Kieselgel 60 F_{254}* plates and *Merck Kieselgel RP-18 60 F_{254}*, and visualized with UV (λ_{max} 254 or 365 nm). UV–Vis spectra were recorded on *Hitachi UV/VIS U-1900* and *Shimadzu PC-160* spectrophotometers. ^{1}H and ^{13}C NMR spectra were acquired on an *Agilent DD2 800* spectrometer at 298 K unless stated otherwise. Chemical shifts (δ) are reported in parts per million (ppm) and referenced to the residual solvent peak (DMSO-d_6: δ_H = 2.50 ppm, δ_C = 39.5 ppm; pyridine-d_5: δ_H = 8.74, 7.58, 7.22 ppm, δ_C = 150.35, 135.91, 123.87 ppm). Coupling constants (*J*) are quoted in Hertz (Hz). The abbreviations s, d, t, m, trbz refer to singlet, doublet, triplet, multiplet and tribenzoporphyrazine phenyl ring protons, respectively. ^{1}H and ^{13}C resonances were assigned unambiguously based on ^{1}H-^{1}H COSY, ^{1}H-^{13}C HSQC, and ^{1}H-^{13}C HMBC experiments. FT-IR spectra were recorded on *Bruker IR* spectrometer, in the range 500–4000 cm^{-1} with KBr as a blank. Mass spectra (HRMS ESI) were carried out by the *Advanced Chemical Equipment and Instrumentation Facility at the Faculty of Chemistry*, *Wielkopolska Center for Advanced Technologies at Adam Mickiewicz University in Poznan* and *Department of Inorganic and Analytical Chemistry at Poznan University of Medical Sciences*.

Tribenzoporphyrazine **1** was synthesized according to reference [41].

3.2. Synthesis

3.2.1. 22,23-Bis(4-(3,5-dibutoxycarbonylphenoxy)butylsulfanyl)tribenzo-[b,g,l]-22,23-dioxo-22,23-seco-porphyrazinato magnesium(II) (2)

The synthetic method was adapted from [15]. Tribenzoporphyrazine **1** (42 mg, 0.034 mmol) was dissolved in CH_2Cl_2 (30 mL) in a round-bottom flask open to the air. A solution of $KMnO_4$ (6 mg, 0.038 mmol in 30 mL of water) was added and the reaction mixture was stirred vigorously in the dark for 2 h. After that, the organic layer was separated in a separatory funnel. CH_2Cl_2 was evaporated under reduced pressure, and the blue residue was chromatographed on silica gel, using CH_2Cl_2, and later, CH_2Cl_2:methanol 20:1 (v/v) as eluents to give **2** in the form of a blue film (14.5 mg, 34% yield). M.p. 151–153 °C. R_f (CH_2Cl_2/methanol 20:1 v/v) 0.12. UV–Vis ($CHCl_3$): λ_{max}, nm (logε) 319 (4.88), 337 (4.89), 369 (4.83), 621 (4.61), 670 (4.54), 727 (4.97). ^{1}H NMR (800 MHz, pyridine-d_5): δ 9.68–9.54 (m, 5H, trbz-H), 8.66–7.72 (m, 13H, trbz-H, isophthal-H), 4.40–4.29, 4.14–4.07 (2 × m, 12H, 2 × $\underline{CH_2}$O), 2.37–2.01 (m, 4H, $\underline{SCH_2}$), 1.61, 1.42 (2 × m, 8H, 2 × $\underline{CH_2}CH_2CH_3$), 1.34, 1.19 (2 × m, 8H, 2 × $\underline{CH_2}CH_2CH_3$), 1.31–1.22 (m, 8H, $SCH_2\underline{CH_2CH_2}$), 0.85, 0.76 (2 × t, J = 7 Hz, 12H, 2 × CH_3); ^{13}C NMR (201 MHz, pyridine-d_5): δ 168.0, 167.4, 161.9, 152.6, 143.1, 143.0, 142.1, 138.2, 135.0, 133.6, 133.2, 126.5, 126.2, 125.4, 125.2, 124.6, 122.2, 121.1, 67.8, 67.5, 34.5, 33.9, 33.3, 33.1, 21.8, 21.7, 21.7, 16.2, 16.2. FT-IR (KBr, ν_{max}/cm^{-1}): 2943, 2924, 2850, 1724, 1684, 1558, 1522, 1506, 1458, 1310, 1306, 1238, 932. HRMS (ESI) *m/z* found: 1279.3926, $[M+H]^+$, $C_{68}H_{71}MgN_8O_{12}S_2$ requires 1279.4483; 1317.3404, $[M+K]^+$ $C_{68}H_{70}MgN_8O_{12}S_2K$ requires 1317.4042; 2596.7021, $[2M+K]^+$ $C_{136}H_{140}Mg_2N_{16}O_{24}S_4K$ requires 2595.8447. HPLC purity is provided in the supplementary information.

3.2.2. 22,23-Bis[4-(3,5-dibutoxycarbonylphenoxy)butylsulfanyl]tribenzo-[b,g,l]porphyrazine (3)

Pz **1** (66 mg, 0.053 mmol) was suspended in 3 mL of trifluoroacetic acid in a round bottomed flask. Reaction mixture was stirred in the dark for 15 min in air. Afterwards, reaction mixture was poured on ice and neutralized with $NaHCO_3$. Blue product was extracted with dichloromethane. Organic layer was collected and the solvent was evaporated to dryness giving solid residue, which was purified by means of column chromatography using silica gel and eluents CH_2Cl_2, later CH_2Cl_2:methanol 100:1 to 50:1 (v/v) to give 30.5 mg of deep blue film identified as **3** (yield 47%). M.p. 137–139 °C. R_f (CH_2Cl_2) 0.29. UV–Vis (CH_2Cl_2): λ_{max}, nm (logε) 319 (4.02), 338 (4.05), 614 (3.90), 704 (4.13). ^{1}H NMR (800 MHz, pyridine-d_5) δ 9.26 (s, 2H, trbz), 9.16 (s, 2H, trbz), 9.07 (d, J = 5.5 Hz, 1H, trbz), 9.02 (d, J = 5.5 Hz, 1H, trbz), 8.62 (m, 2H, 4′ isophthalate), 8.24 (m, 2H, trbz), 8.09 (m, 4H, trbz), 8.02 (m, 4H, 2′(6′) isophthalate), 4.39 (m, 8H, −COOCH_2−), 4.11 (m, 4H, Ar−O−CH_2), 3.94 (m, 4H, S−CH_2), 2.06 (m, 4H, S−CH_2−CH_2−$\underline{CH_2}$), 1.92 (m, 4H, S−CH_2−$\underline{CH_2}$), 1.66 (m, 8H, −$\underline{CH_2}$−CH_2−CH_3), 1.38 (m,

8H, $-\underline{CH_2}-CH_3$), 0.87 (m, 12H, CH_3), −1.85 (s, 2H, 2 × NH). ^{13}C NMR (201 MHz, pyridine-d_5) δ 166.3, 165.6, 160.3, 159.5, 150.7, 140.6, 139.3, 136.5, 133.3, 132.6, 132.5, 132.3, 131.1, 130.6, 124.4, 123.6, 123.4, 123.3, 123.1, 122.8, 120.5, 119.7, 69.4, 66.0, 62.2, 31.4, 30.5, 26.9, 20.0, 14.4. FT-IR (KBr, ν_{max}/cm^{-1}): 3292 (NH), 2959, 2926, 2870, 1719, 1684, 1558, 1506, 1456, 1387, 1339, 1314, 1238, 1119, 1055, 1024, 993, 875, 760, 739, 669. HRMS (ESI) *m/z* found: 1224.5420, $[M]^+$ $C_{68}H_{72}N_8O_{10}S_2$ requires 1224.4813; 1225.6148, $[M+H]^+$ $C_{68}H_{73}N_8O_{10}S_2$ requires 1225.4891; 1247.5799, $[M+Na]^+$ $C_{68}H_{72}N_8O_{10}S_2Na$ requires 1247.4711. For HPLC purity, see supplementary information.

3.3. Singlet oxygen measurements and spectroscopic studies

Singlet oxygen generation by *seco*-porphyrazine **2** was measured in DMF according to the methodology described previously and using the indirect chemical method with DPBF [38,54,55]. 1,3-Diphenylisobenzofuran (DPBF) was used as a singlet oxygen chemical quencher (*Aldrich*). Unsubstituted zinc phthalocyanine (ZnPc) with a known singlet oxygen quantum yield (0.56 in DMF) was used as a reference [56].

3.4. Liposome preparation

1-Palmitoyl-2-oleoyl-*sn-glycero*-3-phosphocholine (POPC), L-α-phosphatidyl-DL-glycerol (chicken egg, PG) 1,2-dioleoyl-3-trimethylammonium-propane (chloride salt, DOTAP) and 1,2-dioleoyl-*sn-glycero*-3-phosphoethanolamine (DOPE) were purchased from *Avanti Polar Lipids Inc*. Four different liposome formulations were prepared by a thin-film hydration method [32,46]. Briefly, appropriate amounts of the lipid stock solutions in chloroform (POPC – 25 mg/mL, PG – 25 mg/mL, DOPE – 25 mg/mL, DOTAP – 10 mg/mL) and the photosensitizer (0.4 mg/mL) were placed in glass tubes, mixed and evaporated to dryness using a rotary evaporator. Films formed on the bottom of glass tubes were dried overnight in a vacuum oven at room temperature to evaporate any remaining chloroform. Subsequently, the dried films were hydrated with HEPES buffered saline (10 mM HEPES (N-(2-hydroxyethyl)piperazine-N'-(2-ethanesulfonic acid)), 140 mM NaCl, pH = 7.5), and dispersed by vortexing for 5–10 min. The resulting liposome suspensions were passed 21 times through polycarbonate membranes with a pore diameter of 100 nm, using a syringe extruder (*Avanti Polar Lipids Inc*) to obtain unilamellar liposomes with a uniform size distribution. The molar ratios of ingredients in the final liposome formulations were: (*i*) **2** (0.1), PG (2), POPC (8); (*ii*) **2** (0.1), DOTAP (2), POPC (8); (*iii*) **2** (0.1), PG (2), DOPE (8); (*iv*) **2** (0.1), DOTAP (2), DOPE (8). The liposome size was determined by dynamic light scattering measurements using a *Beckman Coulter N4 Plus Particle Size Analyzer* (see supplementary information 4.1). Samples were stored at 2–8 °C under argon and were protected from light. The final concentration of photosensitizer achieved in the liposome suspensions was 100 μM. These suspensions were diluted with DME medium without FBS to achieve appropriate concentration for biological activity evaluation on cultured cells. Liposomes without photosensitizers were prepared as controls.

3.5. Biological activity against cancer cell lines

3.5.1. Cell Culture

Oral squamous cell carcinoma cell lines derived from the tongue (CAL 27, HSC-3) were purchased from *ATCC* (CAL 27) or provided by Dr. R. Kramer (*University of California, San Francisco, UCSF, USA*) (HSC-3) [57]. Human cervical epithelial adenocarcinoma cells (HeLa) were purchased from *ATCC*. Cells were cultured in Dulbecco's modified Eagle medium (DMEM) supplemented with 10% (v/v) heat-inactivated fetal bovine serum (FBS), penicillin (100 U/mL), streptomycin (100 μg/mL) and L-glutamine (4 mM) (DMEM/10). Cells were incubated in T-25 tissue culture flasks at 37 °C in a humidified atmosphere containing 5% CO_2 and were passaged 1:6 (HSC-3, HeLa) or 1:4 (CAL 27) twice a week using a Trypsin-EDTA solution (UCSF). All media, penicillin-streptomycin solution, L-glutamine, FBS, Trypsin-EDTA, phosphate-buffered saline (PBS), Dulbecco's phosphate-buffered saline (DPBS), were obtained from the *UCSF Cell Culture Facility, San Francisco, USA*. Photosensitizers were dissolved in dimethyl sulfoxide (DMSO, *Sigma-Aldrich*) and subsequently diluted in DMEM (without FBS and phenol red) to obtain the desired concentration of photosensitizer used in the experiments. The DMSO concentration in the final solution did not exceed 0.25%.

3.5.2. Dark Toxicity

One day before the experiment, cells were seeded in 48-well plates at a density 1.8 × 10^5 in 1 mL of medium (with FBS and phenol red) and used at approximately 80% confluence. Subsequently, cells were washed with PBS (1.0 mL) and 1 mL of medium without FBS and phenol red, containing the photosensitizer at a given concentration, was added to each well, except controls. The FBS-free media were used to avoid binding of photosensitizers to serum proteins. After the 24 h incubation at 37 °C, cells were washed with PBS, 1 mL of complete medium was added to each well, and the cells were incubated for 24 h at 37 °C. Cell viability was quantified by the Alamar Blue assay. Cells incubated either with medium alone or medium/0.25% DMSO served as controls.

3.5.3. Light-dependent toxicity

One day before the experiment CAL 27, HSC-3 or HeLa cells were seeded in 48-well plates at a density 1.8 × 10^5 cells per well, respectively, in 1 mL of complete medium, and used at approximately 80% confluence. Cells were washed with PBS (1 mL), and 1 mL of medium without FBS and phenol red, containing a photosensitizer, was added to each well, except controls. The cells were incubated for 24 h at 37 °C, washed with PBS and irradiated for 20 min with light of wavelength 690 nm from a *High Power LED Multi Chip Emitter* (*Roithner Lasertechnik GmbH*, 9.8 V). The light intensity at the surface of the plate was set to 3.0 mW/cm^2 measured by a *Thorlabs TM100A Optical Power Meter,* and the total light dose was 3.6 J/cm^2. One plate from each experiment was not exposed to light and served as a control. Directly after light exposure, medium without FBS and phenol red was replaced with 1 mL of complete medium, and the cells were incubated for 24 h at 37 °C. Cell viability was quantified by the Alamar Blue assay.

3.5.4. Cell Viability

Cell morphology was evaluated by *Nikon TMS* inverted phase-contrast microscopy at 100× magnification. The number of viable cells used for the experiments was determined by the Trypan Blue exclusion assay (*Gibco-Invitrogen Corporation*). Cell viability was quantified by a modified Alamar Blue assay [58,59]. Briefly, 1.0 mL of 10% (v/v) Alamar Blue dye in the appropriate complete medium was added to each well. After incubation at 37 °C for 2–3 h, 200 μL of the supernatant was assayed by measuring the absorbance at 570 nm and 600 nm. Cell viability (as a percentage of control cells) was calculated according to the formula:

$$\text{Cell viability} = [(A_{570} - A_{600}) \text{ of test cells}] \times 100/[(A_{570} - A_{600}) \text{ of control cells}].$$

3.5.5. Statistical analysis

Statistical analyses were performed with one-way analysis of variance ANOVA followed by Dunnett's multiple comparison test using *GraphPad Prism version 6.07 for Windows, GraphPad Software, San Diego California, USA*. The results were presented as the means ± SD from experiments performed in triplicate. A probability value (p) of less than 0.05 was considered significantly different.

4. Conclusions

A new member of the *seco*-porphyrazine group, namely S-*seco*-Pz, was obtained, and its physicochemical properties and photocytotoxicity were examined. Heating a mixture of an aqueous alkaline solution of sodium hydroxide and a solution of 22,23-bis[4-(3,5-dibutoxycarbonylphenoxy)butylsulfanyl]tribenzo[b,g,l]porphyrazinato magnesium(II) in dichloromethane resulted in the formation of novel S-*seco*-Pz. The optimization of the synthesis procedure resulted in a 34% yield of the target macrocycle, following the biphasic system consisting of an aqueous $KMnO_4$ solution and Pz substrate in dichloromethane. Physicochemical characterization of the S-*seco*-Pz was performed with the use of NMR spectroscopy, UV–Vis spectroscopy, as well as mass spectrometry. Singlet oxygen quantum yield generation measurements following an indirect chemical method with 1,3-diphenylisobenzofuran in DMF revealed that the novel S-*seco*-Pz efficiently mediates singlet oxygen generation to a moderate extent ($\Phi_\Delta = 0.27$), indicating a five-fold increase over the parent molecule.

The potential utility of S-*seco*-porphyrazine in photodynamic therapy was assessed by measuring its photocytotoxicity *in vitro* on three cell lines. The macrocycle was non-toxic in the dark (cell viability > 80%). After irradiation with 690 nm light, the calculated IC_{50} were 0.61, 0.18 and 4.1 μM for CAL 27, HSC-3 and HeLa cells, respectively. Four different liposomal compositions, two of them neutral, one negatively and one positively charged were applied in the photocytotoxicity study. Overall, the cationic liposomes exhibited the best efficiency, as the IC_{50} values were the lowest for CAL 27 and HeLa cells (0.24 and 0.31 μM, respectively), while for HSC-3 the IC_{50} value was slightly higher (0.25 μM), than those for the free Pz **2**. However, the cytotoxicity of **Pz 2** in PG:POPC and PG:DOPE liposomes was much lower than that of the the free compound. Thus, optimal liposome compositions should be established for novel photosensitizers.

All these results indicate that the new *seco*-tribenzoporphyrazine can be regarded as a potential photosensitizer for use in photodynamic therapy of cancer, along with the developed cationic liposomal nanocarrier.

Declaration of Competing Interest

The authors declare that they have no known competing financial interests or personal relationships that could have appeared to influence the work reported in this paper.

Acknowledgments

This study was supported by the National Science Centre, Poland under Grant No. 2016/21/B/NZ9/00783. The authors thank Beata Kwiatkowska and Rita Kuba for excellent technical assistance. Authors thank Eliza Matuszewska, MSc and Jan Matysiak DSc, Ph.D. for mass spectra measurements using the AB Sciex LC/MS/MS System API 4000 QTRAP. DTM would like to thank Agata Kaluzna-Mlynarczyk, for her generous support.

Appendix A. Supplementary material

Supplementary data to this article can be found online at https://doi.org/10.1016/j.bioorg.2020.103634.

References

[1] S.L.J. Michel, B.M. Hoffman, S.M. Baum, A.G.M. Barrett, Peripherally functionalized porphyrazines: Novel metallomacrocycles with broad, untapped potential, in: K.D. Karlin (Ed.), Prog. Inorg. Chem. John Wiley & Sons, Inc., New York, USA, 2002, pp. 473–590.

[2] M.J. Fuchter, C. Zhong, H. Zong, B.M. Hoffman, A.G.M. Barrett, Porphyrazines: designer macrocycles by peripheral substituent change, Aust. J. Chem. 61 (2008) 235–255, https://doi.org/10.1071/CH07445.

[3] M.S. Rodríguez-Morgade, P.A. Stuzhin, The chemistry of porphyrazines: an overview, J. Porphyr. Phthalocyanines 08 (2004) 1129–1165, https://doi.org/10.1142/S1088424604000490.

[4] A.A. Brilkina, L.V. Dubasova, E.A. Sergeeva, A.J. Pospelov, N.Y. Shilyagina, N.M. Shakhova, et al., Photobiological properties of phthalocyanine photosensitizers Photosens, Holosens and Phthalosens: A comparative in vitro analysis, J. Photochem. Photobiol., B 191 (2019) 128–134, https://doi.org/10.1016/j.jphotobiol.2018.12.020.

[5] J. Nackiewicz, M. Kliber-Jasik, M. Skonieczna, A novel pro-apoptotic role of zinc octacarboxyphthalocyanine in melanoma me45 cancer cell's photodynamic therapy (PDT), J. Photochem. Photobiol., B 190 (2019) 146–153, https://doi.org/10.1016/j.jphotobiol.2018.12.002.

[6] B. Pucelik, I. Gürol, V. Ahsen, F. Dumoulin, J.M. Dąbrowski, Fluorination of phthalocyanine substituents: Improved photoproperties and enhanced photodynamic efficacy after optimal micellar formulations, Eur. J. Med. Chem. 124 (2016) 284–298, https://doi.org/10.1016/j.ejmech.2016.08.035.

[7] N.S. Mani, L.S. Beall, A.J.P. White, D.J. Williams, A.G.M. Barrett, B.M. Hoffman, Serendipitous desymmetrisation during porphyrazine synthesis: an X-ray crystallographic study of 2,3,7,8,12,13,17,18-octakis(dimethylamino)-2-secoporphyrazine-2,3-dione, J. Chem. Soc., Chem. Commun. (1994) 1943–1944, https://doi.org/10.1039/c39940001943.

[8] S.M. Baum, A.A. Trabanco, A.G. Montalban, A.S. Micallef, C. Zhong, H.G. Meunier, et al., Synthesis and reactions of aminoporphyrazines with annulated five- and seven-membered rings, J. Org. Chem. 68 (2003) 1665–1670, https://doi.org/10.1021/jo026484u.

[9] X. Guinchard, M.J. Fuchter, A. Ruggiero, B.J. Duckworth, A.G.M. Barrett, B.M. Hoffman, Multigram synthesis of a water-soluble porphyrazine and derived *seco*-porphyrazine labeling agents, Org. Lett. 9 (2007) 5291–5294, https://doi.org/10.1021/ol702481x.

[10] A.V. Kozlov, P.A. Stuzhin, New porphyrazinoid containing pyrazine in place of one pyrrole ring, Macroheterocycles 7 (2014) 170–173, https://doi.org/10.6060/mhc140270s.

[11] E.G. Sakellariou, A.G. Montalban, S.L. Beall, D. Henderson, H.G. Meunier, D. Phillips, et al., Novel peripherally functionalized seco-porphyrazines: synthesis, characterization and spectroscopic evaluation, Tetrahedron 59 (2003) 9083–9090, https://doi.org/10.1016/j.tet.2003.09.060.

[12] E.G. Sakellariou, A.G. Montalban, H.G. Meunier, G. Rumbles, D. Phillips, R.B. Ostler, et al., Peripherally metalated secoporphyrazines: a new generation of photoactive pigments, Inorg. Chem. 41 (2002) 2182–2187, https://doi.org/10.1021/ic0111583.

[13] A.G. Montalban, H.G. Meunier, R.B. Ostler, A.G.M. Barrett, B.M. Hoffman, G. Rumbles, Photoperoxidation of a diamino zinc porphyrazine to the *seco*-zinc porphyrazine: Suicide or murder? J. Phys. Chem. A 103 (1999) 4352–4358, https://doi.org/10.1021/jp9905068.

[14] M.J. Fuchter, B.M. Hoffman, A.G.M. Barrett, Ring-opening metathesis polymer sphere-supported *seco* -porphyrazines: efficient and recyclable photooxygenation catalysts, J. Org. Chem. 71 (2006) 724–729, https://doi.org/10.1021/jo052156t.

[15] A.G. Montalban, S.J. Lange, L.S. Beall, N.S. Mani, D.J. Williams, A.J. White, et al., Seco-porphyrazines: synthetic, structural, and spectroscopic investigations, J. Org. Chem. 62 (1997) 9284–9289, https://doi.org/10.1021/jo971599x.

[16] A. Nazli, E. Gonca, A. Gül, Partially oxidized porphyrazines, J. Porphyr. Phthalocyanines 10 (2006) 996–1002, https://doi.org/10.1142/S108842460600034X.

[17] E. Gonca, Ü.G. Baklaci, H.A. Dinçer, Seco-porphyrazines with eight (p-tolyl) and (o-tolyl) units, J. Porphyr. Phthalocyanines 12 (2008) 116–122, https://doi.org/10.1142/S1088424608000157.

[18] M. Altunkaya, E. Gonca, Synthesis and characterization of new soluble fluorinated seco-porphyrazines, Polyhedron 30 (2011) 1035–1039, https://doi.org/10.1016/j.poly.2011.01.003.

[19] E. Gonca, Synthesis and characterization of Octakis(4-biphenyl)-2- *seco* -2,3-Dioxoporphyrazinato iron derivatives, Synth. React. Inorg., Met.-Org., Nano-Met. Chem. 45 (2015) 779–783, https://doi.org/10.1080/15533174.2013.843558.

[20] E. Gonca, B. Keskin, Synthesis and characterization of soluble *seco* -porphyrazines with bulky substituents, J. Coord. Chem. 62 (2009) 2875–2882, https://doi.org/10.1080/00958970902962220.

[21] E. Gonca, Ü.G. Baklacı, H.A. Dinçer, Synthesis and spectral properties of novel seco-porphyrazines with eight 4-biphenyl groups, Polyhedron 27 (2008) 2431–2435, https://doi.org/10.1016/j.poly.2008.04.025.

[22] I. Sugita, S. Shimizu, T. Fukuda, N. Kobayashi, Nickel and palladium complexes of seco-tribenzoporphyrazines derived from one-pot condensation of 1,3-diiminoisoindoline, Tetrahedron Lett. 54 (2013) 1599–1601, https://doi.org/10.1016/j.tetlet.2013.01.057.

[23] V.N. Nemykin, A.E. Polshyna, E.A. Makarova, N. Kobayashi, E.A. Lukyanets, Unexpected formation of the nickel seco-tribenzoporphyrazine with a tribenzotetraazachlorin-type absorption spectrum, Chem. Commun. 48 (2012) 3650–3652, https://doi.org/10.1039/c2cc30760j.

[24] H. Nie, C.L. Stern, B.M. Hoffman, A.G. Barrett, Decapitation of dihydroporphyrazinediol derivatives: synthesis and X-ray structure of a novel seco-porphyrazine, Chem. Commun. (1999) 703–704, https://doi.org/10.1039/A900555B.

[25] A.A. Trabanco, A.G. Montalban, G. Rumbles, A.G. Barrett, B.M. Hoffman, A seco-porphyrazine: Superb sensitizer for singlet oxygen generation and endoperoxide synthesis, Synlett 2000 (2000) 1010–1012.

[26] T. Yoshida, T. Furuyama, N. Kobayashi, Synthesis and optical properties of tetraazaporphyrin phosphorus(V) complexes with electron-rich heteroatoms, Tetrahedron Lett. 56 (2015) 1671–1674, https://doi.org/10.1016/j.tetlet.2015.02.033.

[27] J. Fernández-Ariza, M. Urbani, M.S. Rodríguez-Morgade, T. Torres, Panchromatic photosensitizers based on push-pull, unsymmetrically substituted porphyrazines, Chem. – Eur. J. 24 (2018) 2618–2625, https://doi.org/10.1002/chem.201705242.
[28] S. Belviso, M. Amati, R. Rossano, A. Crispini, F. Lelj, Non-symmetrical aryl- and arylethynyl-substituted thioalkyl-porphyrazines for optoelectronic materials: synthesis, properties, and computational studies, Dalton Trans. 44 (2015) 2191–2207, https://doi.org/10.1039/C4DT03317E.
[29] M. Falkowski, T. Rebis, J. Piskorz, L. Popenda, S. Jurga, J. Mielcarek, et al., Multiwalled carbon nanotube/sulfanyl porphyrazine hybrids deposited on glassy carbon electrode — effect of nitro peripheral groups on electrochemical properties, J. Porphyr. Phthalocyanines 21 (2017) 295–301, https://doi.org/10.1142/S1088424617500134.
[30] T. Koczorowski, T. Rębiś, W. Szczolko, P. Antecka, A. Teubert, G. Milczarek, et al., Reduced graphene oxide/iron(II) porphyrazine hybrids on glassy carbon electrode for amperometric detection of NADH and L-cysteine, J. Electroanal. Chem. 848 (2019) 113322, https://doi.org/10.1016/j.jelechem.2019.113322.
[31] J. Piskorz, S. Lijewski, M. Gierszewski, K. Gorniak, L. Sobotta, B. Wicher, et al., Sulfanyl porphyrazines: Molecular barrel-like self-assembly in crystals, optical properties and in vitro photodynamic activity towards cancer cells, Dyes Pigments 136 (2017) 898–908, https://doi.org/10.1016/j.dyepig.2016.09.054.
[32] J. Piskorz, D.T. Mlynarczyk, W. Szczolko, K. Konopka, N. Düzgüneş, J. Mielcarek, Liposomal formulations of magnesium sulfanyl tribenzoporphyrazines for the photodynamic therapy of cancer, J. Inorg. Biochem. 184 (2018) 34–41, https://doi.org/10.1016/j.jinorgbio.2018.04.010.
[33] N. Kabay, Y. Baygu, H.K. Alpoguz, A. Kaya, Y. Gök, Synthesis and characterization of porphyrazines as novel extractants for the removal of Ag(I) and Hg(II) from aqueous solution, Dyes Pigments 96 (2013) 372–376, https://doi.org/10.1016/j.dyepig.2012.09.002.
[34] Y. Liu, X. Zhou, Z. Zhang, B. Zhang, K. Deng, Effect of carrier and axial ligand on the photocatalytic activity of cobalt thioporphyrazine, Chin. J. Catal. 38 (2017) 330–336, https://doi.org/10.1016/S1872-2067(16)62580-9.
[35] C. Yang, L. Gao, B. Zhang, Z. Zhang, K. Deng, Uniform zinc thioporphyrazine nanosphere by self-assembly and the photocatalytic performance, J. Porphyr. Phthalocyanines 22 (2018) 868–876, https://doi.org/10.1142/S1088424618500487.
[36] Reaxys https://www.reaxys.com/ (accessed July 24, 2019).
[37] C.S. Velazquez, G.A. Fox, W.E. Broderick, K.A. Andersen, O.P. Anderson, A.G. Barrett, et al., Star-porphyrazines: synthetic, structural, and spectral investigation of complexes of the polynucleating porphyrazineoctathiolato ligand, J. Am. Chem. Soc. 114 (1992) 7416–7424, https://doi.org/10.1021/ja00045a013.
[38] M. Gierszewski, M. Falkowski, L. Sobotta, M. Stolarska, L. Popenda, S. Lijewski, et al., Porphyrazines with peripheral isophthaloxyalkylsulfanyl substituents and their optical properties, J. Photochem. Photobiol. Chem. 307–308 (2015) 54–67, https://doi.org/10.1016/j.jphotochem.2015.04.003.
[39] N. Bellec, A. Garrido Montalban, D.B.G. Williams, A.S. Cook, M.E. Anderson, X. Feng, et al., Porphyrazinediols: synthesis, characterization, and complexation to group IVB metallocenes, J. Org. Chem. 65 (2000) 1774–1779, https://doi.org/10.1021/jo9916840.
[40] E. Güzel, A. Günsel, A.T. Bilgiçli, G.Y. Atmaca, A. Erdoğmuş, M.N. Yarasir, Synthesis and photophysicochemical properties of novel thiadiazole-substituted zinc (II), gallium (III) and silicon (IV) phthalocyanines for photodynamic therapy, Inorganica Chim Acta 467 (2017) 169–176, https://doi.org/10.1016/j.ica.2017.07.058.
[41] D.T. Mlynarczyk, S. Lijewski, M. Falkowski, J. Piskorz, W. Szczolko, L. Sobotta, et al., Dendrimeric sulfanyl porphyrazines: synthesis, physico-chemical characterization, and biological activity for potential applications in photodynamic therapy, ChemPlusChem 81 (2016) 460–470, https://doi.org/10.1002/cplu.201600051.
[42] N. Düzgüneş, J. Piskorz, P. Skupin-Mrugalska, T. Goslinski, J. Mielcarek, K. Konopka, Photodynamic therapy of cancer with liposomal photosensitizers, Ther Deliv 9 (2018) 823–832, https://doi.org/10.4155/tde-2018-0050.
[43] C.S. Jin, G. Zheng, Liposomal nanostructures for photosensitizer delivery, Lasers Surg. Med. 43 (2011) 734–748, https://doi.org/10.1002/lsm.21101.
[44] A. Puri, K. Loomis, B. Smith, J.-H. Lee, A. Yavlovich, E. Heldman, et al., Lipid-based nanoparticles as pharmaceutical drug carriers: from concepts to clinic, Crit. Rev. Ther. Drug Carr. Syst. 26 (2009) 523–580, https://doi.org/10.1615/critrevtherdrugcarriersyst.v26.i6.10.
[45] P. Walde, S. Ichikawa, Enzymes inside lipid vesicles: preparation, reactivity and applications, Biomol. Eng. 18 (2001) 143–177, https://doi.org/10.1016/S1389-0344(01)00088-0.
[46] N. Düzgüneş, Preparation and quantitation of small unilamellar liposomes and large unilamellar reverse-phase evaporation liposomes, Methods Enzymol. 367 (2003) 23–27, https://doi.org/10.1016/S0076-6879(03)67003-5 Elsevier.
[47] J. Piskorz, K. Konopka, N. Düzgüneş, Z. Gdaniec, J. Mielcarek, T. Goslinski, Diazepinoporphyrazines containing peripheral styryl substituents and their promising nanomolar photodynamic activity against oral cancer cells in liposomal formulations, ChemMedChem 9 (2014) 1775–1782, https://doi.org/10.1002/cmdc.201402085.
[48] X. Wang, J. Jin, W. Li, Q. Wang, Y. Han, H. Liu, Differential in vitro sensitivity of oral precancerous and squamous cell carcinoma cell lines to 5-aminolevulinic acid-mediated photodynamic therapy, Photodiagnosis Photodyn. Ther. 29 (2020) 101554, https://doi.org/10.1016/j.pdpdt.2019.08.036.
[49] P.L. Chu, W.A. Shihabuddeen, K.P. Low, D.J.J. Poon, B. Ramaswamy, Z.-G. Liang, et al., Vandetanib sensitizes head and neck squamous cell carcinoma to photodynamic therapy through modulation of EGFR-dependent DNA repair and the tumour microenvironment, Photodiagnosis Photodyn. Ther. 27 (2019) 367–374, https://doi.org/10.1016/j.pdpdt.2019.06.008.
[50] E. Delaey, F. van Laar, D. De Vos, A. Kamuhabwa, P. Jacobs, P. de Witte, A comparative study of the photosensitizing characteristics of some cyanine dyes, J. Photochem. Photobiol., B 55 (2000) 27–36, https://doi.org/10.1016/S1011-1344(00)00021-X.
[51] M. Lapshina, A. Ustyugov, V. Baulin, A. Terentiev, A. Tsivadze, N. Goldshleger, Crown- and phosphoryl-containing metal phthalocyanines in solutions of poly(N-vinylpyrrolidone): Supramolecular organization, accumulation in cells, photo-induced generation of reactive oxygen species, and cytotoxicity, J. Photochem. Photobiol., B 202 (2020) 111722, https://doi.org/10.1016/j.jphotobiol.2019.111722.
[52] A. Kumar, A. Dixit, S. Sahoo, S. Banerjee, A. Bhattacharyya, A. Garai, et al., Crystal structure, DNA crosslinking and photo-induced cytotoxicity of oxovanadium(IV) conjugates of boron-dipyrromethene, J. Inorg. Biochem. 202 (2020) 110817, https://doi.org/10.1016/j.jinorgbio.2019.110817.
[53] M. Olek, J. Kasperski, D. Skaba, R. Wiench, G. Cieślar, A. Kawczyk-Krupka, Photodynamic therapy for the treatment of oral squamous carcinoma—Clinical implications resulting from in vitro research, Photodiagnosis Photodyn. Ther. 27 (2019) 255–267, https://doi.org/10.1016/j.pdpdt.2019.06.012.
[54] M. Durmuş, V. Ahsen, T. Nyokong, Photophysical and photochemical studies of long chain-substituted zinc phthalocyanines, J. Photochem. Photobiol. Chem. 186 (2007) 323–329, https://doi.org/10.1016/j.jphotochem.2006.08.025.
[55] I. Seotsanyana-Mokhosi, N. Kuznetsova, T. Nyokong, Photochemical studies of tetra-2,3-pyridinoporphyrazines, J. Photochem. Photobiol. Chem. 140 (2001) 215–222, https://doi.org/10.1016/S1010-6030(01)00427-0.
[56] A. Ogunsipe, D. Maree, T. Nyokong, Solvent effects on the photochemical and fluorescence properties of zinc phthalocyanine derivatives, J. Mol. Struct. 650 (2003) 131–140, https://doi.org/10.1016/S0022-2860(03)00155-8.
[57] K. Matsumoto, M. Horikoshi, K. Rikimaru, S. Enomoto, A study of an in vitro model for invasion of oral squamous cell carcinoma, J. Oral Pathol. Med. 18 (1989) 498–501, https://doi.org/10.1111/j.1600-0714.1989.tb01350.x.
[58] R.D. Fields, M.V. Lancaster, Dual-attribute continuous monitoring of cell proliferation/cytotoxicity, Am. Biotechnol. Lab. 11 (1993) 48–50.
[59] K. Konopka, E. Pretzer, P.L. Felgner, N. Düzgüneş, Human immunodeficiency virus type-1 (HIV-1) infection increases the sensitivity of macrophages and THP-1 cells to cytotoxicity by cationic liposomes, Biochim. Biophys. Acta BBA – Mol. Cell Res. 1312 (1996) 186–196, https://doi.org/10.1016/0167-4889(96)00033-X.